On the Performance of a BCS-based Inverse Scattering Technique within the first Born Approximation to Invert Limited Scattered Data

L. Poli, G. Oliveri, A. Massa

Abstract

This report proposes some numerical results about a Bayesian Compressive Sampling-based strategy applied to solve an inserve scattering problem within the Born approximation, dealing with limited scattered data. Exploiting the 'a-priori' information on the sparseness of the scatterers, it has been verified the effectiveness of the technique in solving strongly ill-posed problems.

Contents

1 TEST CASE: Square Cylinder, $V = 1$

Goal: show the performances of BCS when dealing with a sparse scatterer

- Number of Views: V
- Number of Measurements: M
- Number of Cells for the Inversion: N
- Number of Cells for the Direct solver: D
- Side of the investigation domain: L

Test Case Description

Direct solver:

- Square domain divided in $\sqrt{D} \times \sqrt{D}$ cells
- Domain side: $L = 3\lambda$
- $D = 1296$ (discretization for the direct solver: $< \lambda/10$)

Investigation domain:

- Square domain divided in $\sqrt{N} \times \sqrt{N}$ cells
- $L = 3\lambda$
- $2ka = 2 \times \frac{2\pi}{\lambda} \times \frac{L\sqrt{2}}{2} = 6\pi\sqrt{2} = 26.65$
- $\#DOF = \frac{(2ka)^2}{2} = \frac{(2\times\frac{2\pi}{\lambda}\times\frac{L\sqrt{2}}{2})^2}{2} = 4\pi^2\left(\frac{L}{\lambda}\right)^2 = 4\pi^2 \times 9 \approx 355.3$
- N scelto in modo da essere vicino a $\#DOF$: $N = 324$ (18×18)

Measurement domain:

- Measurement points taken on a circle of radius $\rho = 3\lambda$
- Full-aspect measurements
- $M \approx 2ka \rightarrow M = 27$

Sources:

- Plane waves
- $V = 1$
- Amplitude $A = 1$
- Frequency: 300 MHz $(\lambda = 1)$

Object:

- Square cylinder of side $\frac{\lambda}{6} = 0.1667$
- $\varepsilon_r \in \{1.5, 2.0, 2.5, 3.0\}$
- $\sigma = 0$ [S/m]

BCS parameters:

- Initial estimate of the noise: $n_0 = 1.0 \times 10^{-3}$
- Convergenze parameter: $\tau = 1.0 \times 10^{-8}$

RESULTS: $\varepsilon_r = 1.5$

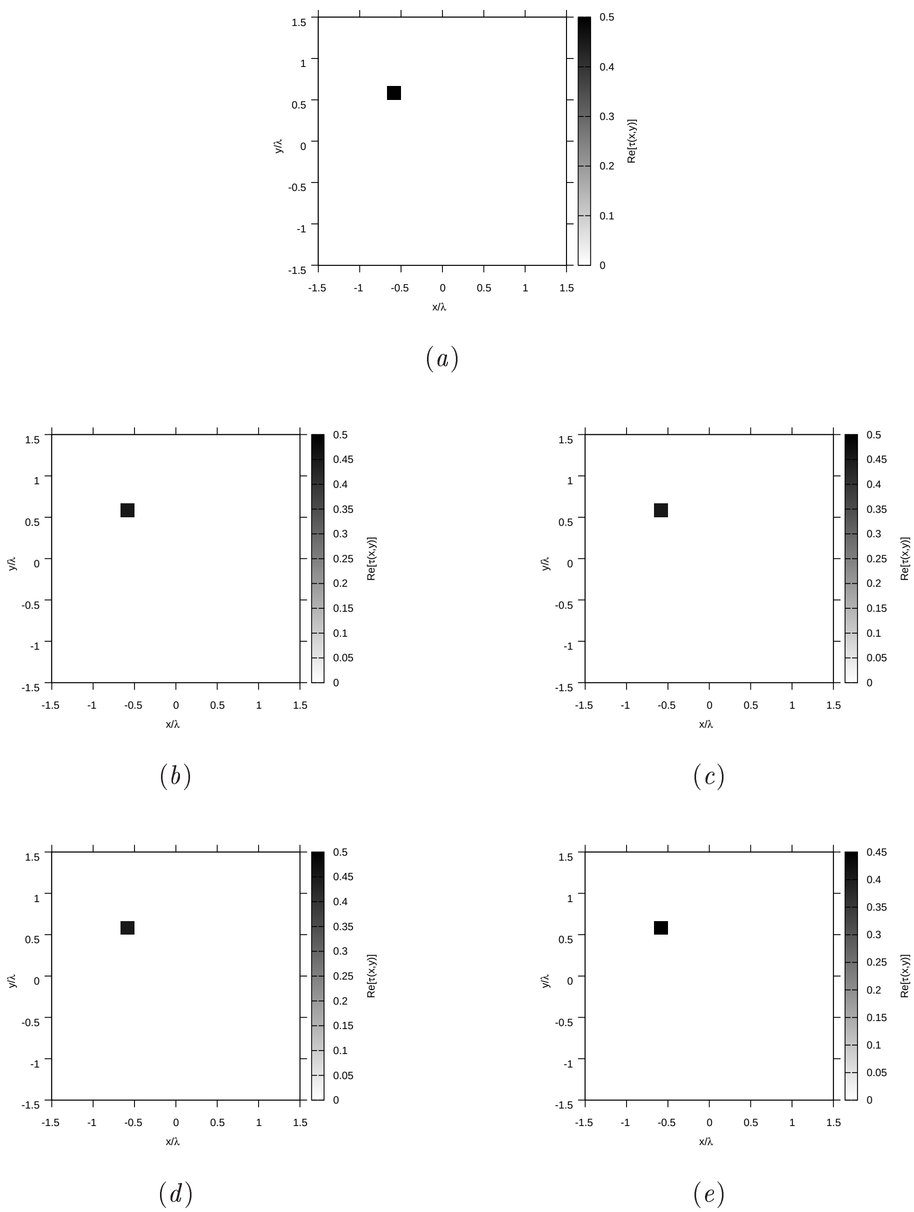

Figure 47. Actual object (a) and BCS reconstructed object for (b) Noiseless case, (c) $SNR = 20$ [dB] , (d) $SNR = 10$ [dB] , (e) $SNR = 5$ [dB].

Observations:

Ricostruzioni molto buone per tutti i valori di SNR.

RESULTS: $\varepsilon_r = 2.0$

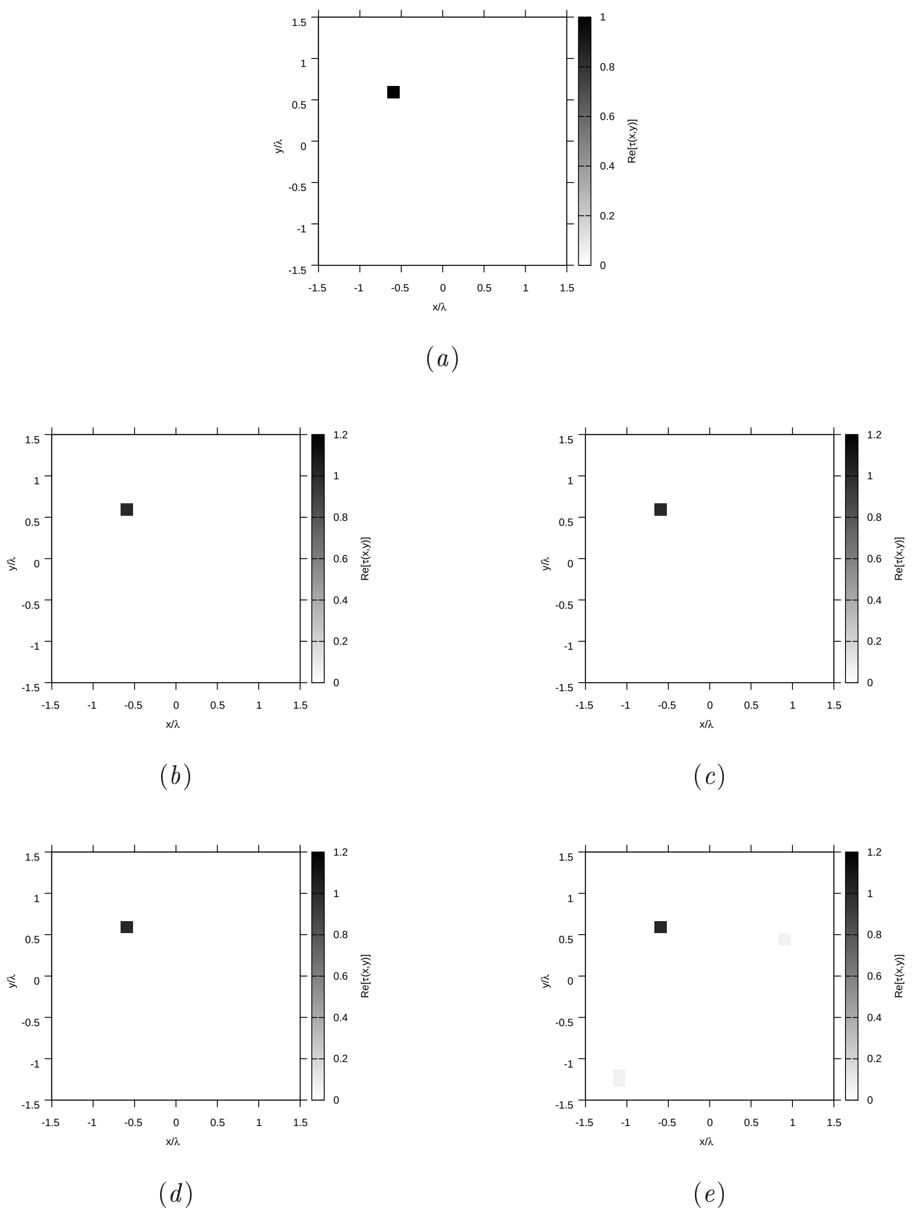

Figure 48. Actual object (a) and BCS reconstructed object for (b) Noiseless case, (c) $SNR = 20$ [dB] , (d) $SNR = 10$ [dB] , (e) $SNR = 5$ [dB].

Observations:

Ricostruzioni molto buone per i valori di SNR fino a $10\,dB$.

RESULTS: $\varepsilon_r = 2.5$

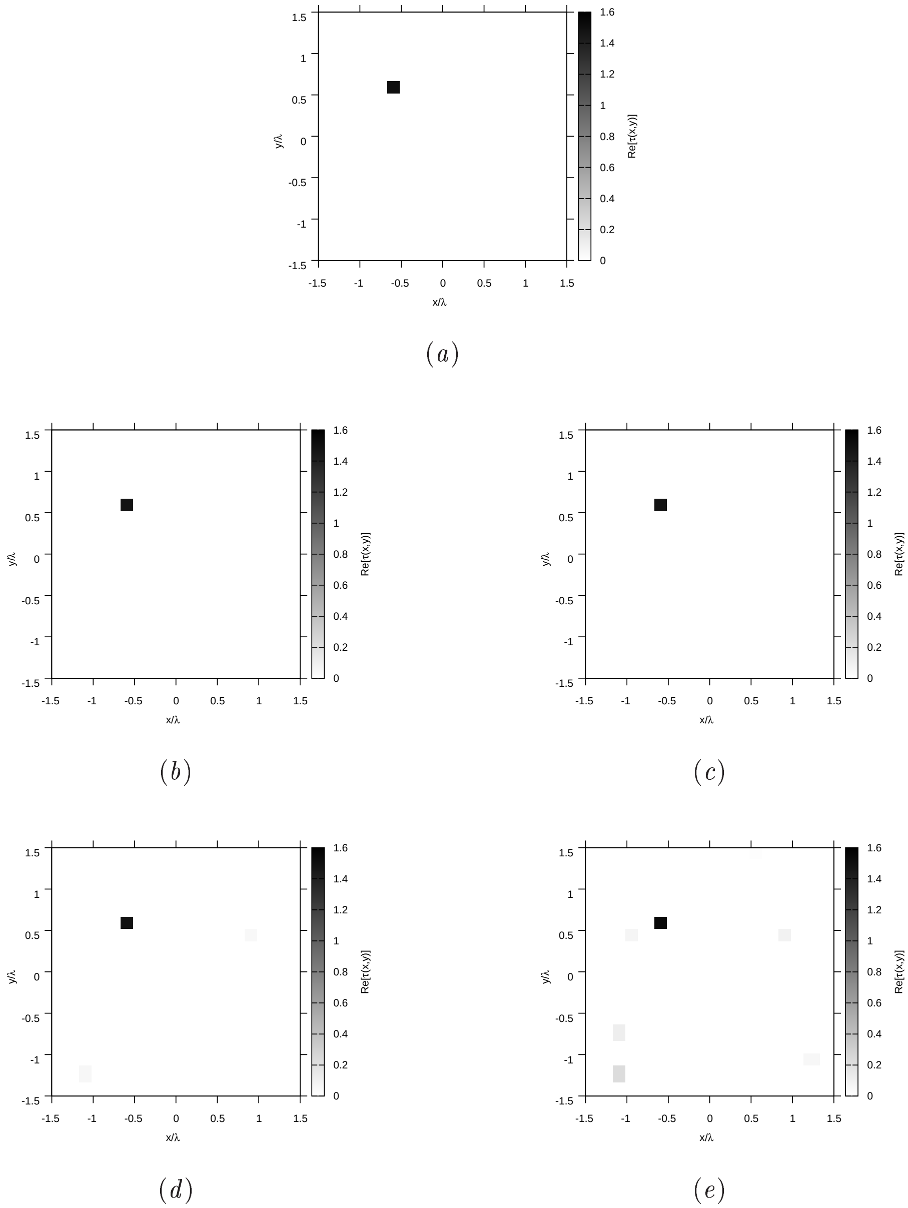

Figure 49. Actual object (a) and BCS reconstructed object for (b) Noiseless case, (c) $SNR = 20$ [dB] , (d) $SNR = 10$ [dB] , (e) $SNR = 5$ [dB].

Observations:

Ricostruzioni molto buone per i casi Noiseless e $SNR = 20\,dB$.

RESULTS: $\varepsilon_r = 3.0$

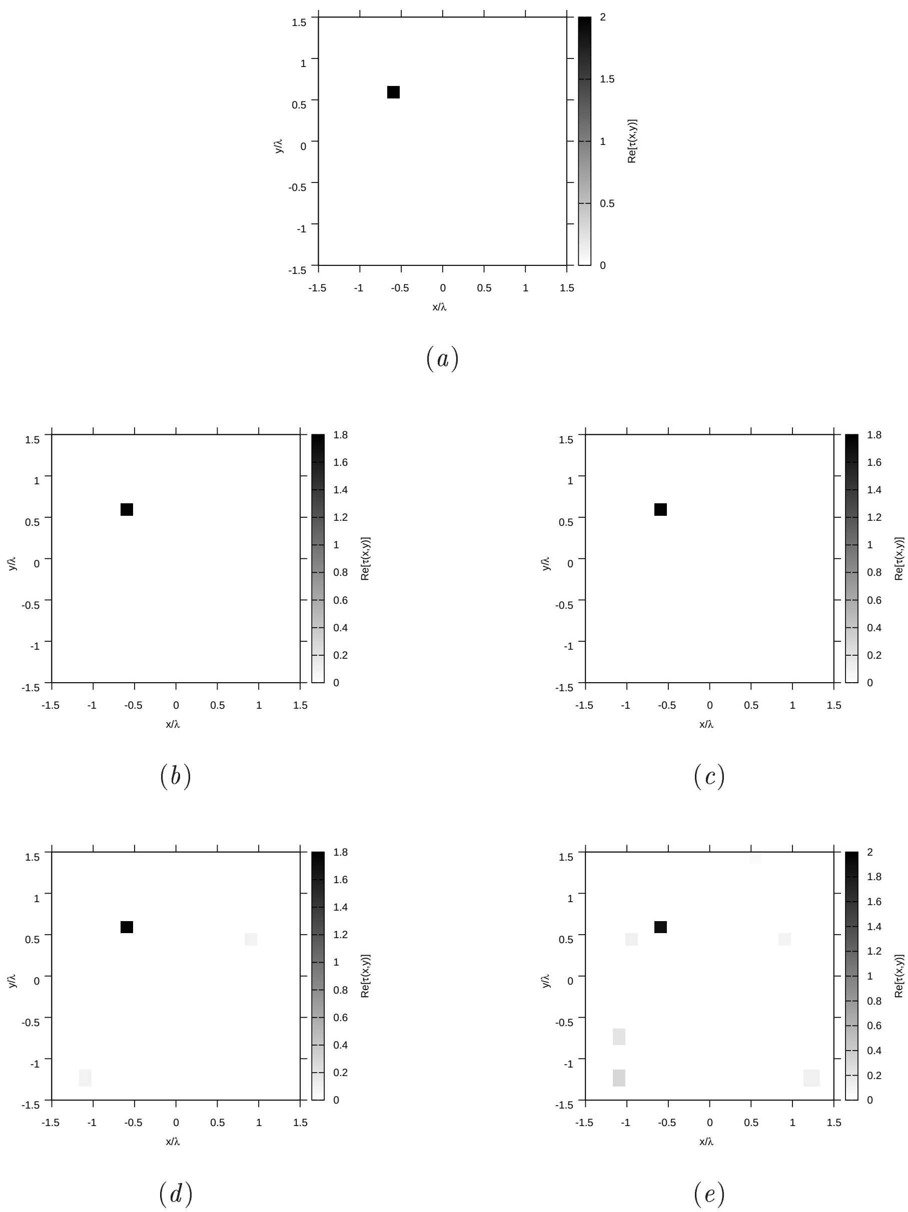

Figure 50. Actual object (a) and BCS reconstructed object for (b) Noiseless case, (c) $SNR = 20$ [dB] , (d) $SNR = 10$ [dB] , (e) $SNR = 5$ [dB].

Observations:

Ricostruzioni molto buone per i casi Noiseless e $SNR = 20\,dB$.

RESULTS: Error Figures

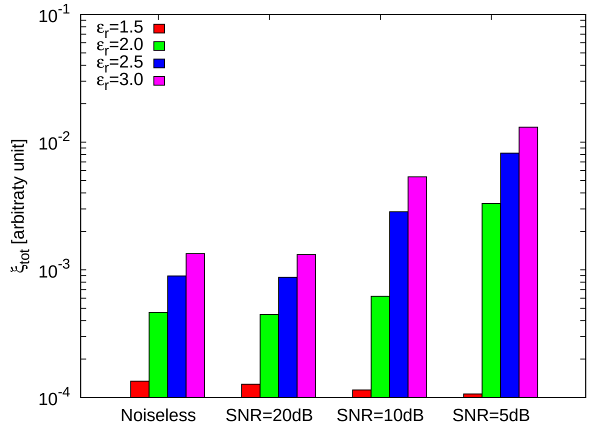

(a)

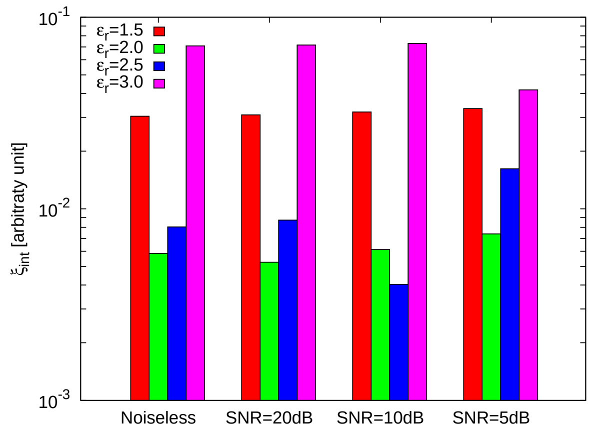

(b)

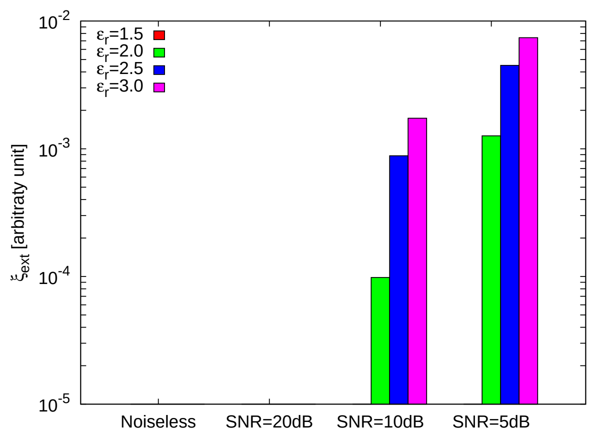

(c)

Figure 51. Behaviour of error figures as a function of ε_r, for different SNR values: (a) total error ξ_{tot}, (b) internal error ξ_{int}, (c) external error ξ_{ext}.

2 TEST CASE: Two Square Cylinders - $V = 1$

Goal: show the performances of BCS when dealing with a sparse scatterer

- Number of Views: V
- Number of Measurements: M
- Number of Cells for the Inversion: N
- Number of Cells for the Direct solver: D
- Side of the investigation domain: L

Test Case Description

Direct solver:

- Square domain divided in $\sqrt{D} \times \sqrt{D}$ cells
- Domain side: $L = 3\lambda$
- $D = 1296$ (discretization for the direct solver: $< \lambda/10$)

Investigation domain:

- Square domain divided in $\sqrt{N} \times \sqrt{N}$ cells
- $L = 3\lambda$
- $2ka = 2 \times \frac{2\pi}{\lambda} \times \frac{L\sqrt{2}}{2} = 6\pi\sqrt{2} = 26.65$
- $\#DOF = \frac{(2ka)^2}{2} = \frac{(2\times\frac{2\pi}{\lambda}\times\frac{L\sqrt{2}}{2})^2}{2} = 4\pi^2\left(\frac{L}{\lambda}\right)^2 = 4\pi^2 \times 9 \approx 355.3$
- N scelto in modo da essere vicino a $\#DOF$: $N = 324$ (18×18)

Measurement domain:

- Measurement points taken on a circle of radius $\rho = 3\lambda$
- Full-aspect measurements
- $M \approx 2ka \rightarrow M = 27$

Sources:

- Plane waves
- $V = 1$
- Amplitude $A = 1$
- Frequency: 300 MHz ($\lambda = 1$)

Object:

- Three square cylinders of side $\frac{\lambda}{6} = 0.1667$
- $\varepsilon_r \in \{1.5, 2.0, 2.5, 3.0\}$ (one square), $\varepsilon_r = 1.9$ (one square)
- $\sigma = 0$ [S/m]

BCS parameters:

- Initial estimate of the noise: $n_0 = 1.0 \times 10^{-3}$
- Convergenze parameter: $\tau = 1.0 \times 10^{-8}$

RESULTS: $\varepsilon_r = 1.5$

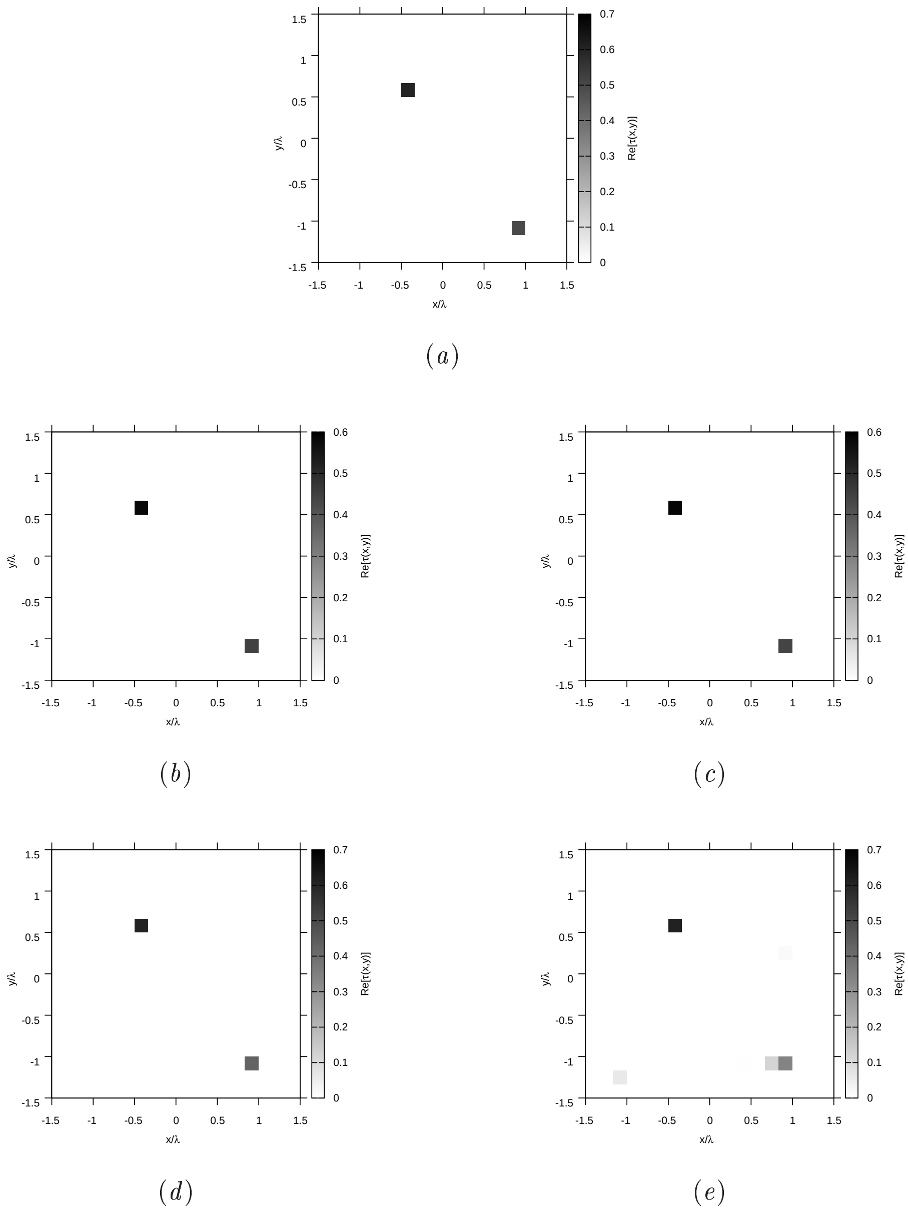

Figure 52. Actual object (a) and BCS reconstructed object for (b) Noiseless case, (c) $SNR = 20$ [dB] , (d) $SNR = 10$ [dB] , (e) $SNR = 5$ [dB].

Observations:

Ricostruzioni molto buone per i valori di SNR fino a $10\,dB$.

RESULTS: $\varepsilon_r = 2.0$

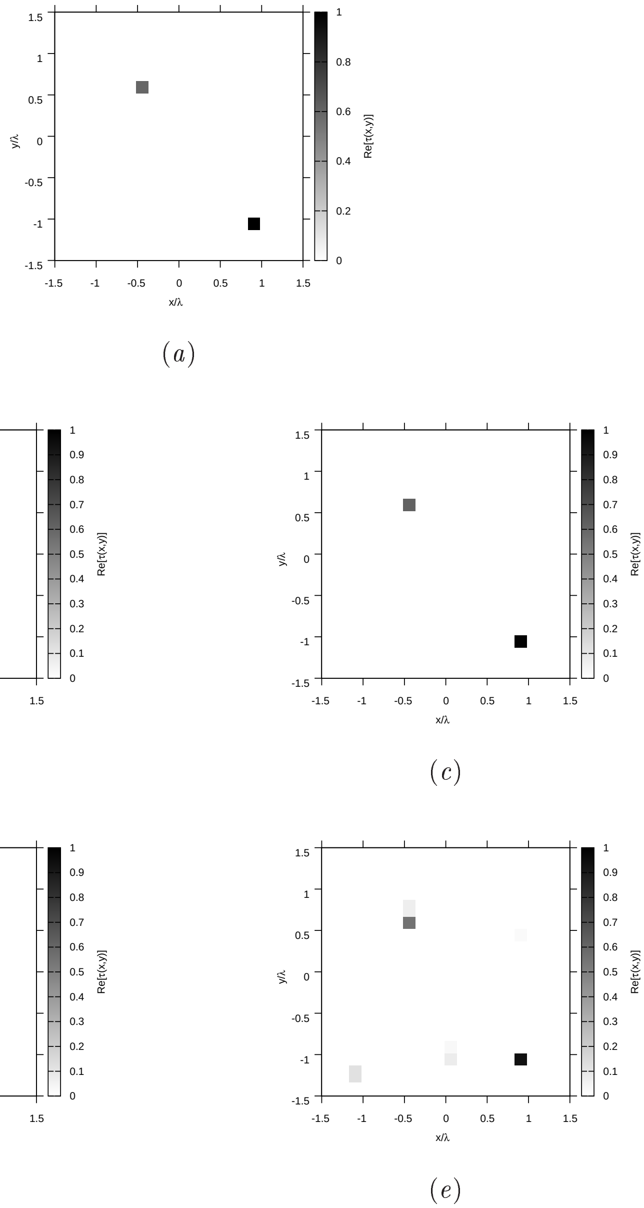

Figure 53. Actual object (a) and BCS reconstructed object for (b) Noiseless case, (c) $SNR = 20$ [dB] , (d) $SNR = 10$ [dB] , (e) $SNR = 5$ [dB].

Observations:

Ricostruzioni molto buone per i valori di SNR fino a $10\,dB$.

RESULTS: $\varepsilon_r = 2.5$

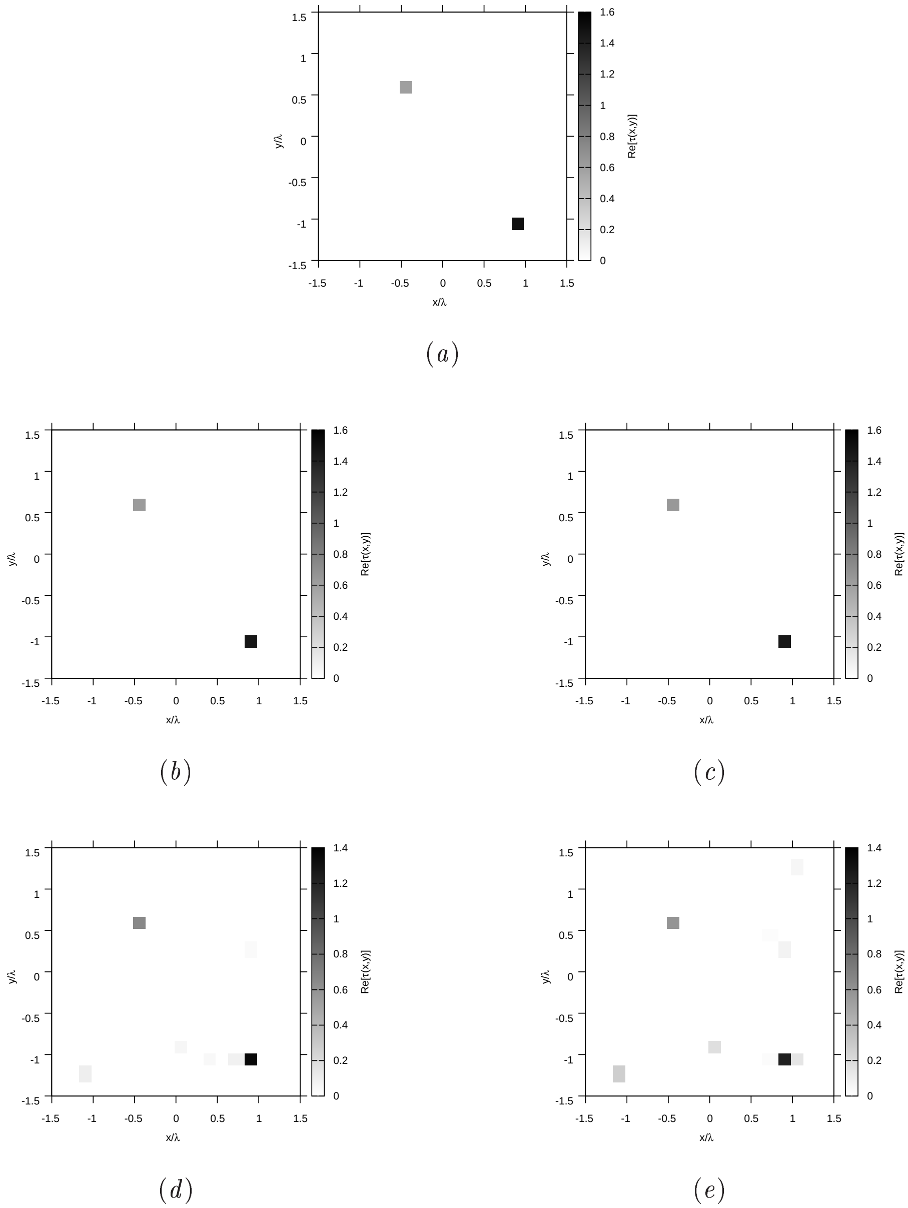

Figure 54. Actual object (a) and BCS reconstructed object for (b) Noiseless case, (c) $SNR = 20$ [dB] , (d) $SNR = 10$ [dB] , (e) $SNR = 5$ [dB].

Observations:

Ricostruzioni molto buone per i casi Noiseless e $SNR = 20\,dB$.

RESULTS: $\varepsilon_r = 3.0$

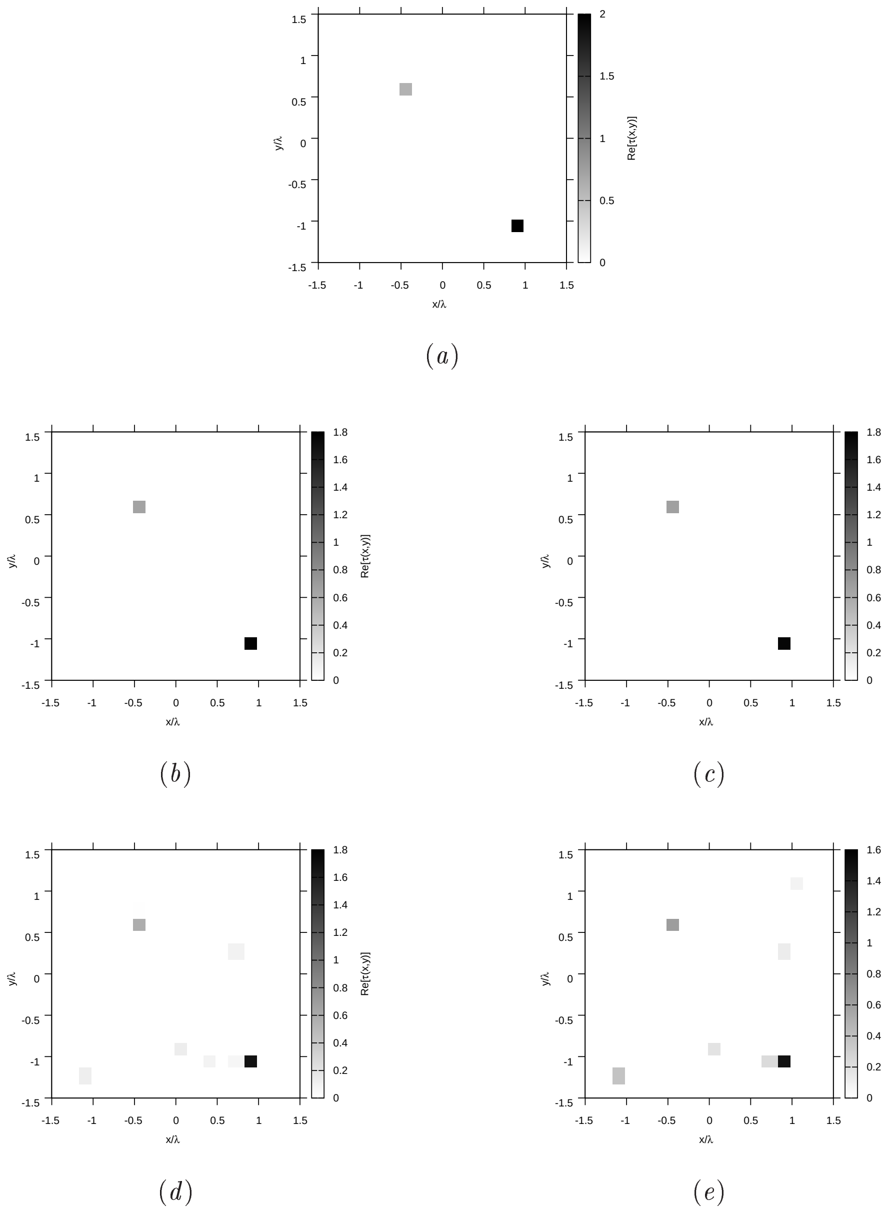

Figure 55. Actual object (a) and BCS reconstructed object for (b) Noiseless case, (c) $SNR = 20$ [dB] , (d) $SNR = 10$ [dB] , (e) $SNR = 5$ [dB].

Observations:

Ricostruzioni molto buone per i casi Noiseless e $SNR = 20\,dB$.

RESULTS: Error Figures

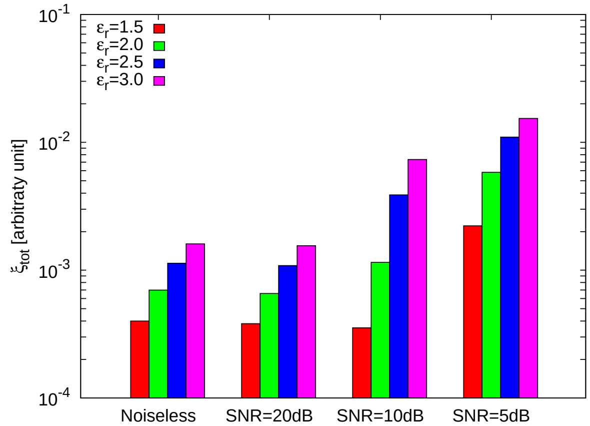

(a)

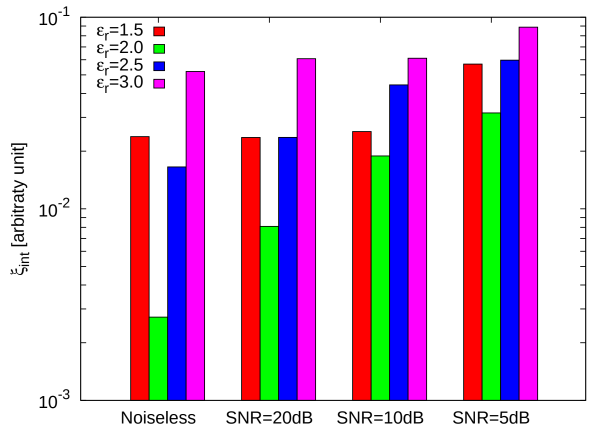

(b)

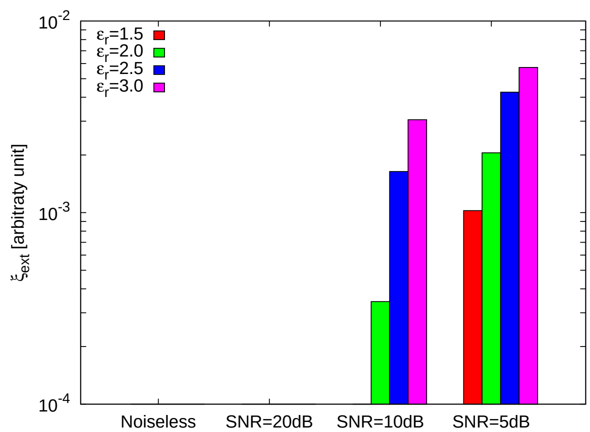

(c)

Figure 56. Behaviour of error figures as a function of ε_r, for different SNR values: (a) total error ξ_{tot}, (b) internal error ξ_{int}, (c) external error ξ_{ext}.

3 TEST CASE: Three Square Cylinders - $V = 1$

Goal: show the performances of BCS when dealing with a sparse scatterer

- Number of Views: V
- Number of Measurements: M
- Number of Cells for the Inversion: N
- Number of Cells for the Direct solver: D
- Side of the investigation domain: L

Test Case Description

Direct solver:

- Square domain divided in $\sqrt{D} \times \sqrt{D}$ cells
- Domain side: $L = 3\lambda$
- $D = 1296$ (discretization for the direct solver: $< \lambda/10$)

Investigation domain:

- Square domain divided in $\sqrt{N} \times \sqrt{N}$ cells
- $L = 3\lambda$
- $2ka = 2 \times \frac{2\pi}{\lambda} \times \frac{L\sqrt{2}}{2} = 6\pi\sqrt{2} = 26.65$
- $\#DOF = \frac{(2ka)^2}{2} = \frac{(2\times\frac{2\pi}{\lambda}\times\frac{L\sqrt{2}}{2})^2}{2} = 4\pi^2\left(\frac{L}{\lambda}\right)^2 = 4\pi^2 \times 9 \approx 355.3$
- N scelto in modo da essere vicino a $\#DOF$: $N = 324$ (18×18)

Measurement domain:

- Measurement points taken on a circle of radius $\rho = 3\lambda$
- Full-aspect measurements
- $M \approx 2ka \rightarrow M = 27$

Sources:

- Plane waves
- $V = 1$
- Amplitude $A = 1$
- Frequency: 300 MHz ($\lambda = 1$)

Object:

- Three square cylinders of side $\frac{\lambda}{6} = 0.1667$
- $\varepsilon_r \in \{1.5, 2.0, 2.5, 3.0\}$ (two squares), $\varepsilon_r = 1.9$ (one square)
- $\sigma = 0$ [S/m]

BCS parameters:

- Initial estimate of the noise: $n_0 = 1.0 \times 10^{-3}$
- Convergenze parameter: $\tau = 1.0 \times 10^{-8}$

RESULTS: $\varepsilon_r = 1.5$

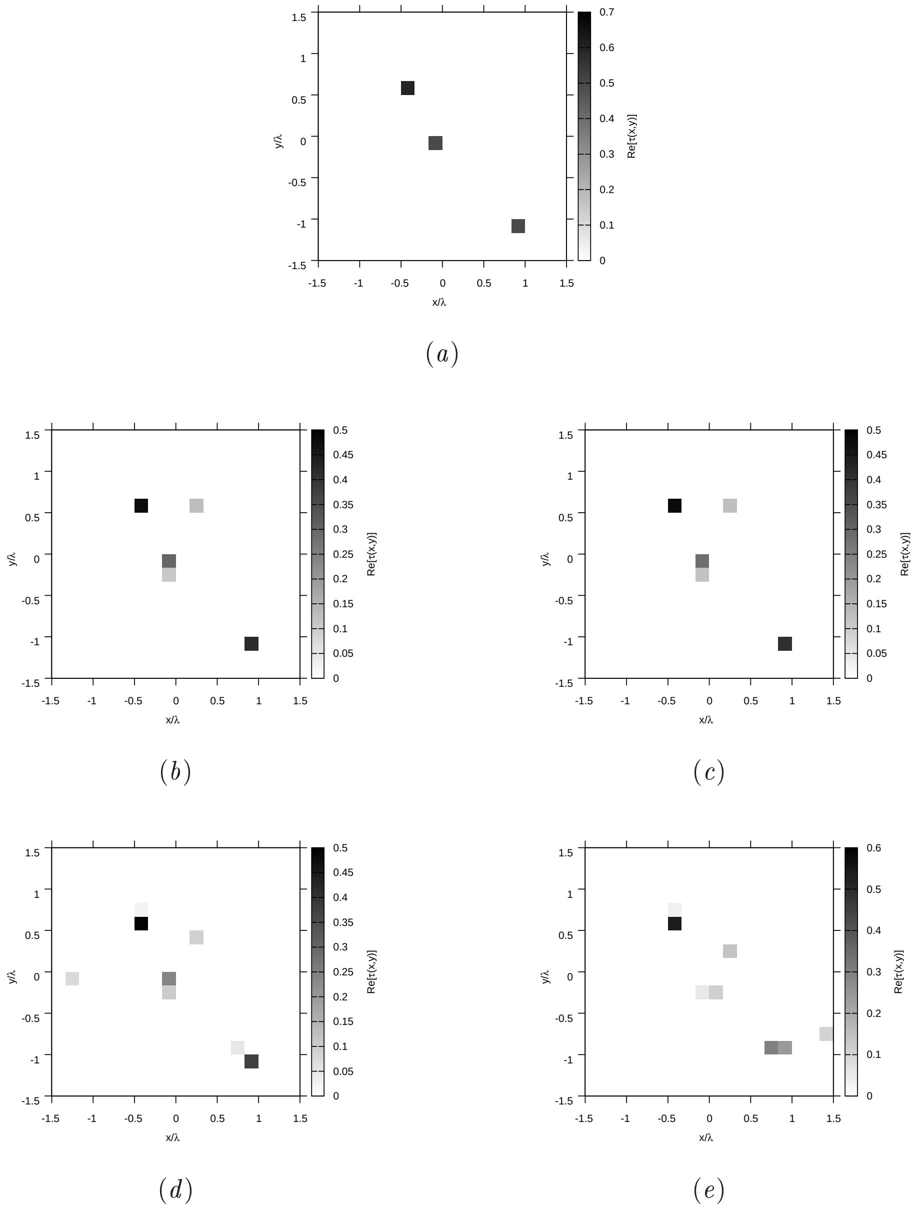

Figure 57. Actual object (a) and BCS reconstructed object for (b) Noiseless case, (c) $SNR = 20$ [dB] , (d) $SNR = 10$ [dB] , (e) $SNR = 5$ [dB].

Observations:

Ricostruzioni non buone in generale.

RESULTS: $\varepsilon_r = 2.0$

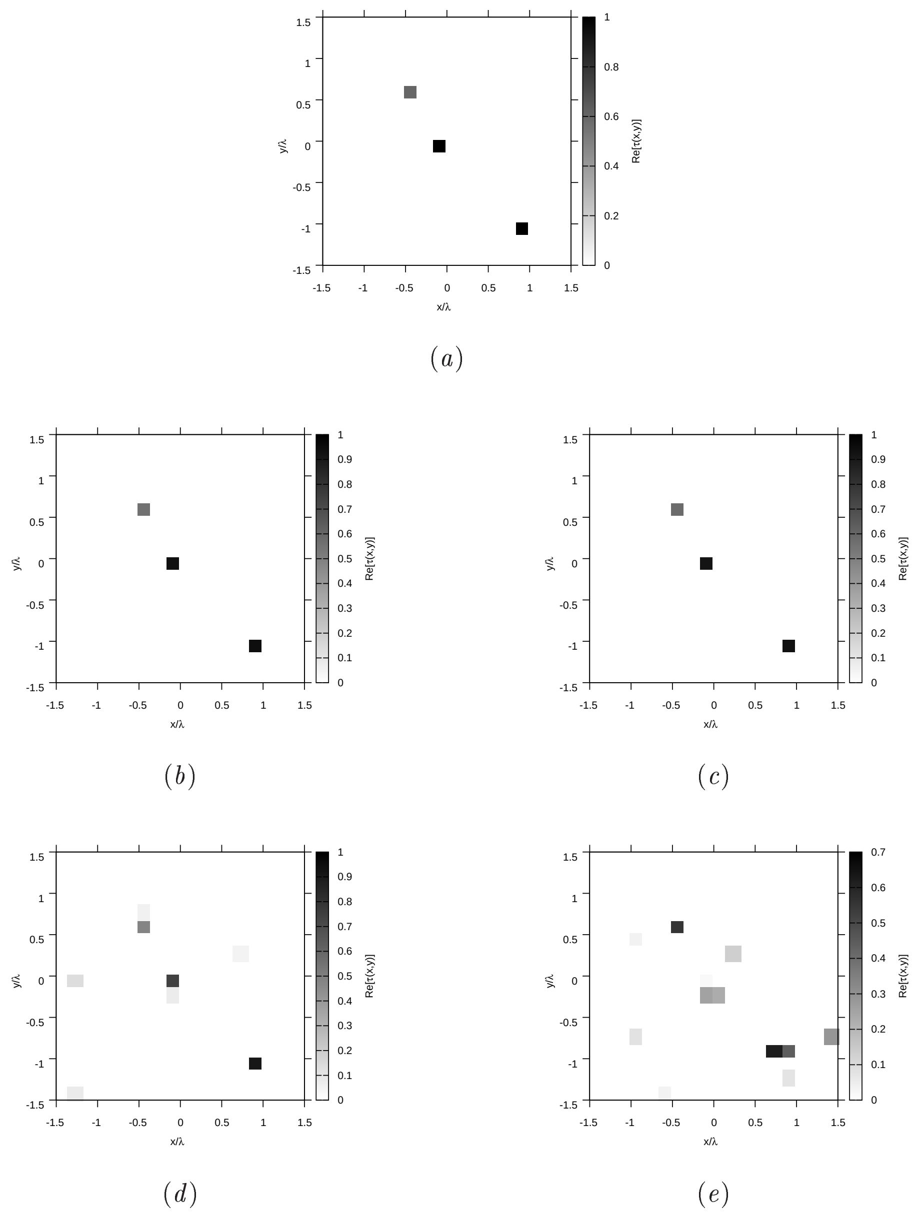

Figure 58. Actual object (a) and BCS reconstructed object for (b) Noiseless case, (c) $SNR = 20$ [dB] , (d) $SNR = 10$ [dB] , (e) $SNR = 5$ [dB].

Observations:

Ricostruzioni molto buone per i casi Noiseless e $SNR = 20\,dB$.

RESULTS: $\varepsilon_r = 2.5$

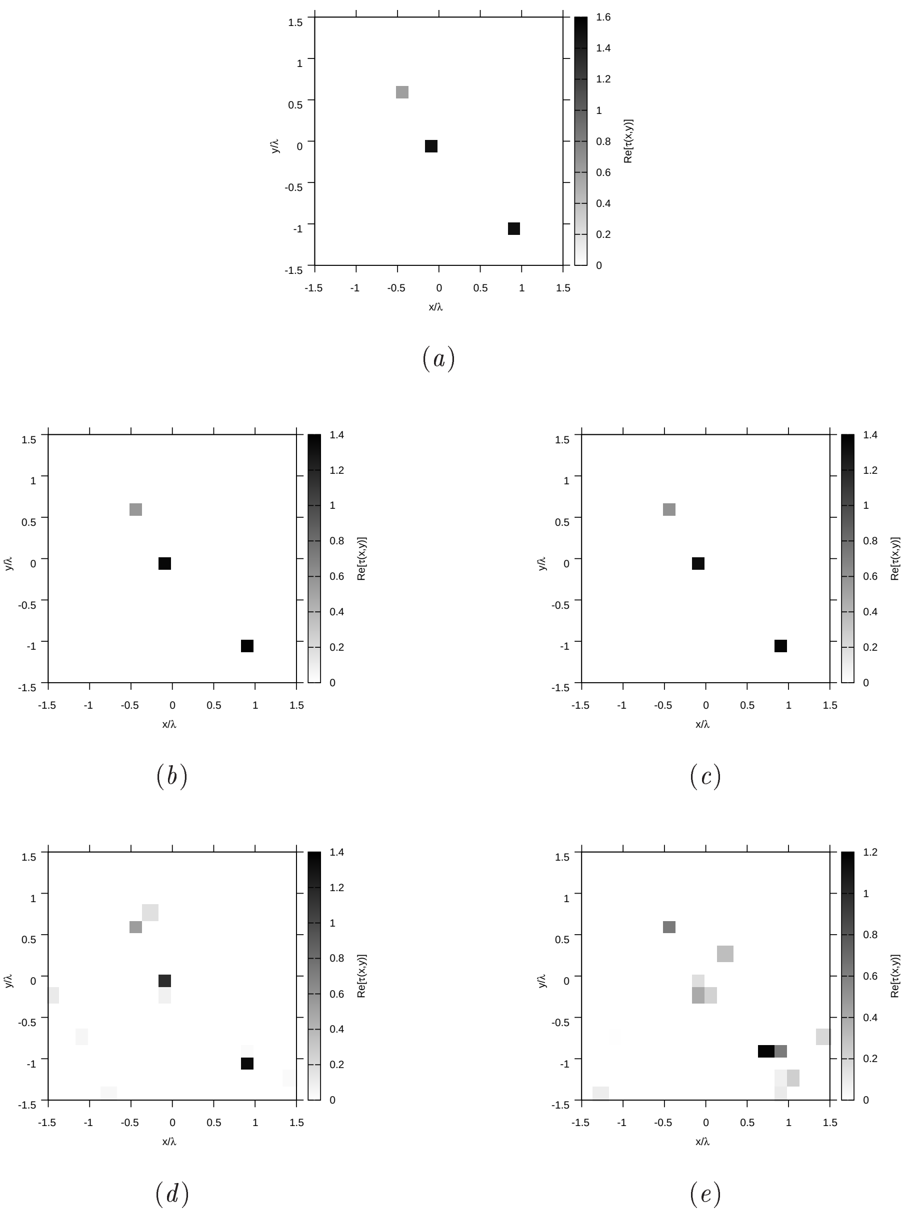

Figure 59. Actual object (a) and BCS reconstructed object for (b) Noiseless case, (c) $SNR = 20$ [dB] , (d) $SNR = 10$ [dB] , (e) $SNR = 5$ [dB].

Observations:

Ricostruzioni molto buone per i casi Noiseless e $SNR = 20\,dB$.

RESULTS: $\varepsilon_r = 3.0$

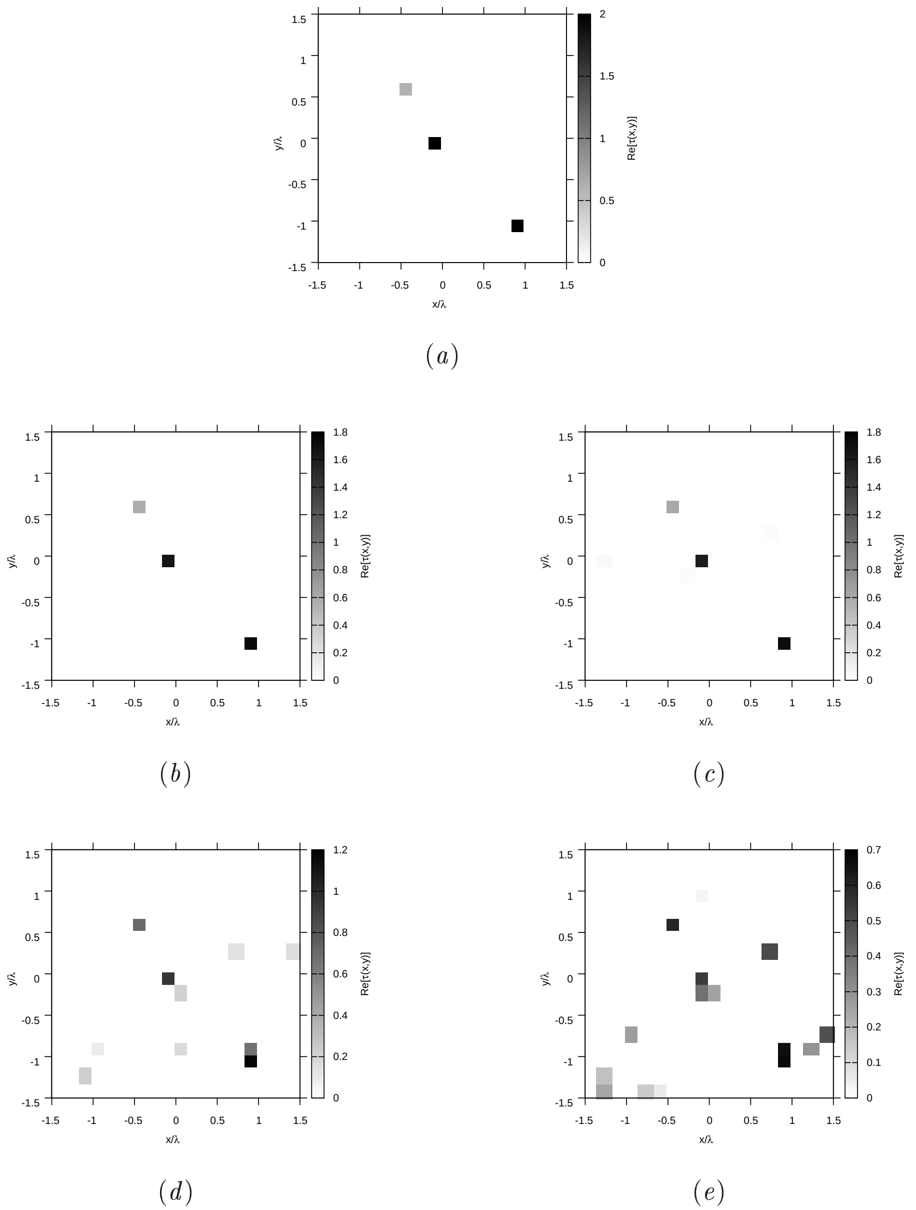

Figure 60. Actual object (a) and BCS reconstructed object for (b) Noiseless case, (c) $SNR = 20$ [dB] , (d) $SNR = 10$ [dB] , (e) $SNR = 5$ [dB].

Observations:

Ricostruzioni molto buone per i casi Noiseless e $SNR = 20\,dB$.

RESULTS: Error Figures

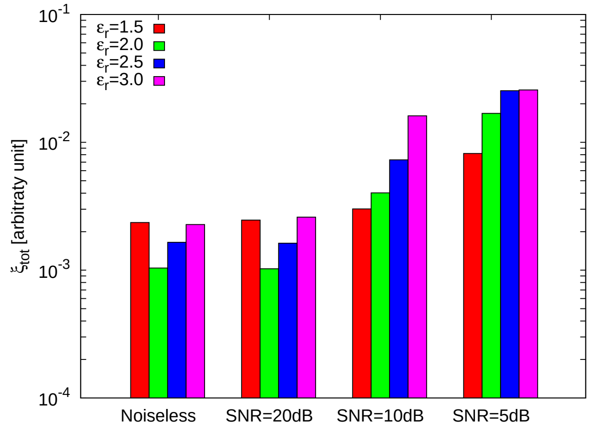

(a)

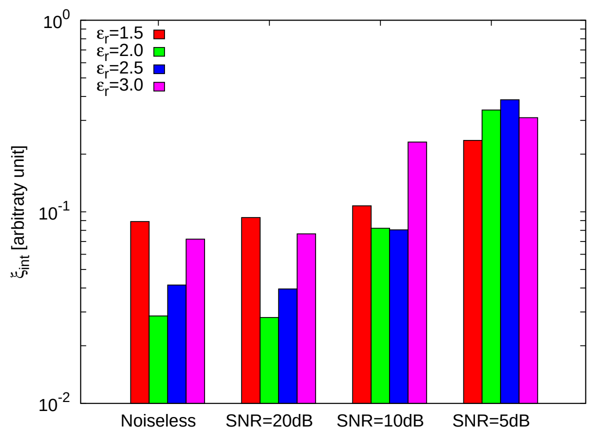

(b)

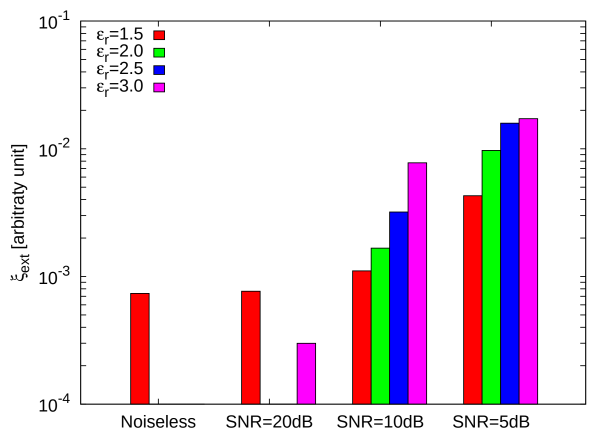

(c)

Figure 61. Behaviour of error figures as a function of ε_r, for different SNR values: (a) total error ξ_{tot}, (b) internal error ξ_{int}, (c) external error ξ_{ext}.

4 TEST CASE: Four Square Cylinders, $V = 1$

Goal: show the performances of BCS when dealing with a sparse scatterer

- Number of Views: V
- Number of Measurements: M
- Number of Cells for the Inversion: N
- Number of Cells for the Direct solver: D
- Side of the investigation domain: L

Test Case Description

Direct solver:

- Square domain divided in $\sqrt{D} \times \sqrt{D}$ cells
- Domain side: $L = 3\lambda$
- $D = 1296$ (discretization for the direct solver: $< \lambda/10$)

Investigation domain:

- Square domain divided in $\sqrt{N} \times \sqrt{N}$ cells
- $L = 3\lambda$
- $2ka = 2 \times \frac{2\pi}{\lambda} \times \frac{L\sqrt{2}}{2} = 6\pi\sqrt{2} = 26.65$
- $\#DOF = \frac{(2ka)^2}{2} = \frac{(2\times\frac{2\pi}{\lambda}\times\frac{L\sqrt{2}}{2})^2}{2} = 4\pi^2\left(\frac{L}{\lambda}\right)^2 = 4\pi^2 \times 9 \approx 355.3$
- N scelto in modo da essere vicino a $\#DOF$: $N = 324$ (18×18)

Measurement domain:

- Measurement points taken on a circle of radius $\rho = 3\lambda$
- Full-aspect measurements
- $M \approx 2ka \rightarrow M = 27$

Sources:

- Plane waves
- $V = 1$
- Amplitude $A = 1$
- Frequency: 300 MHz ($\lambda = 1$)

Object:

- Square cylinder of side $\frac{\lambda}{6} = 0.1667$
- $\varepsilon_r \in \{1.5, 2.0, 2.5, 3.0\}$ (two squares), $\varepsilon_r = 1.9$ (two square)
- $\sigma = 0$ [S/m]

BCS parameters:

- Initial estimate of the noise: $n_0 = 1.0 \times 10^{-3}$
- Convergenze parameter: $\tau = 1.0 \times 10^{-8}$

RESULTS: $\varepsilon_r = 1.5$

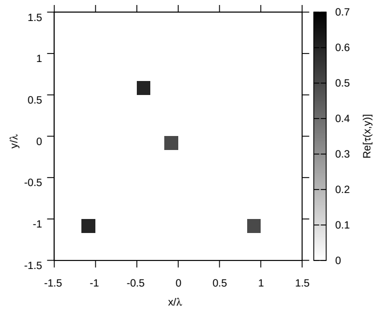

(a)

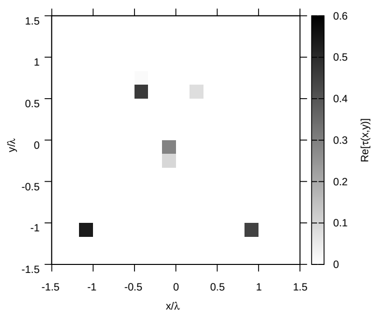

(b)

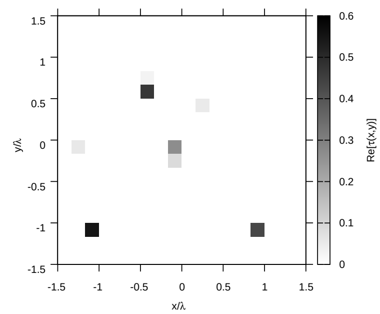

(c)

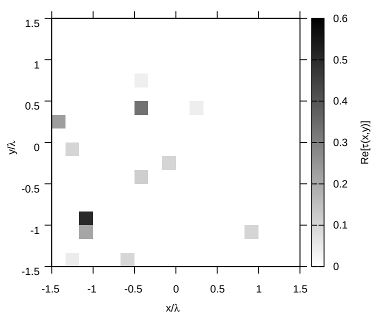

(d)

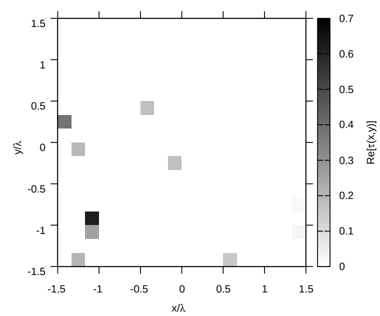

(e)

Figure 62. Actual object (a) and BCS reconstructed object for (b) Noiseless case, (c) $SNR = 20$ [dB] , (d) $SNR = 10$ [dB] , (e) $SNR = 5$ [dB].

Observations:

Ricostruzioni non buone in generale.

RESULTS: $\varepsilon_r = 2.0$

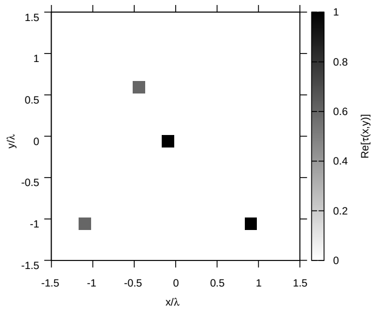

(a)

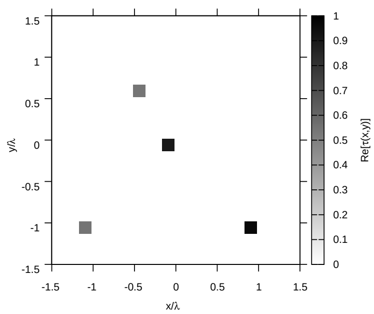

(b)

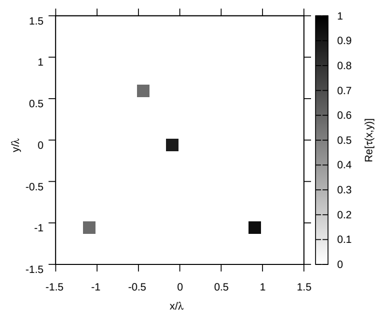

(c)

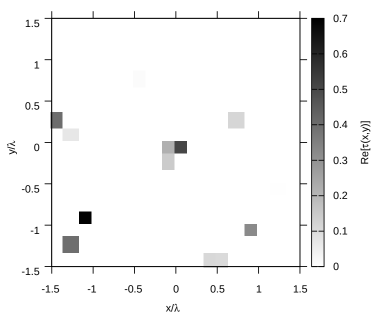

(d)

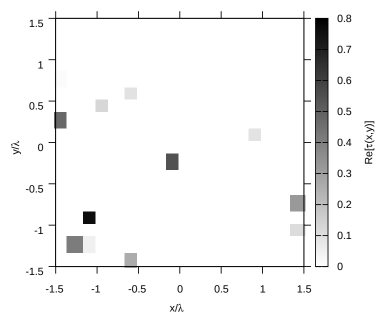

(e)

Figure 63. Actual object (a) and BCS reconstructed object for (b) Noiseless case, (c) $SNR = 20$ [dB] , (d) $SNR = 10$ [dB] , (e) $SNR = 5$ [dB].

Observations:

Ricostruzioni molto buone per i casi Noiseless e $SNR = 20\,dB$.

RESULTS: $\varepsilon_r = 2.5$

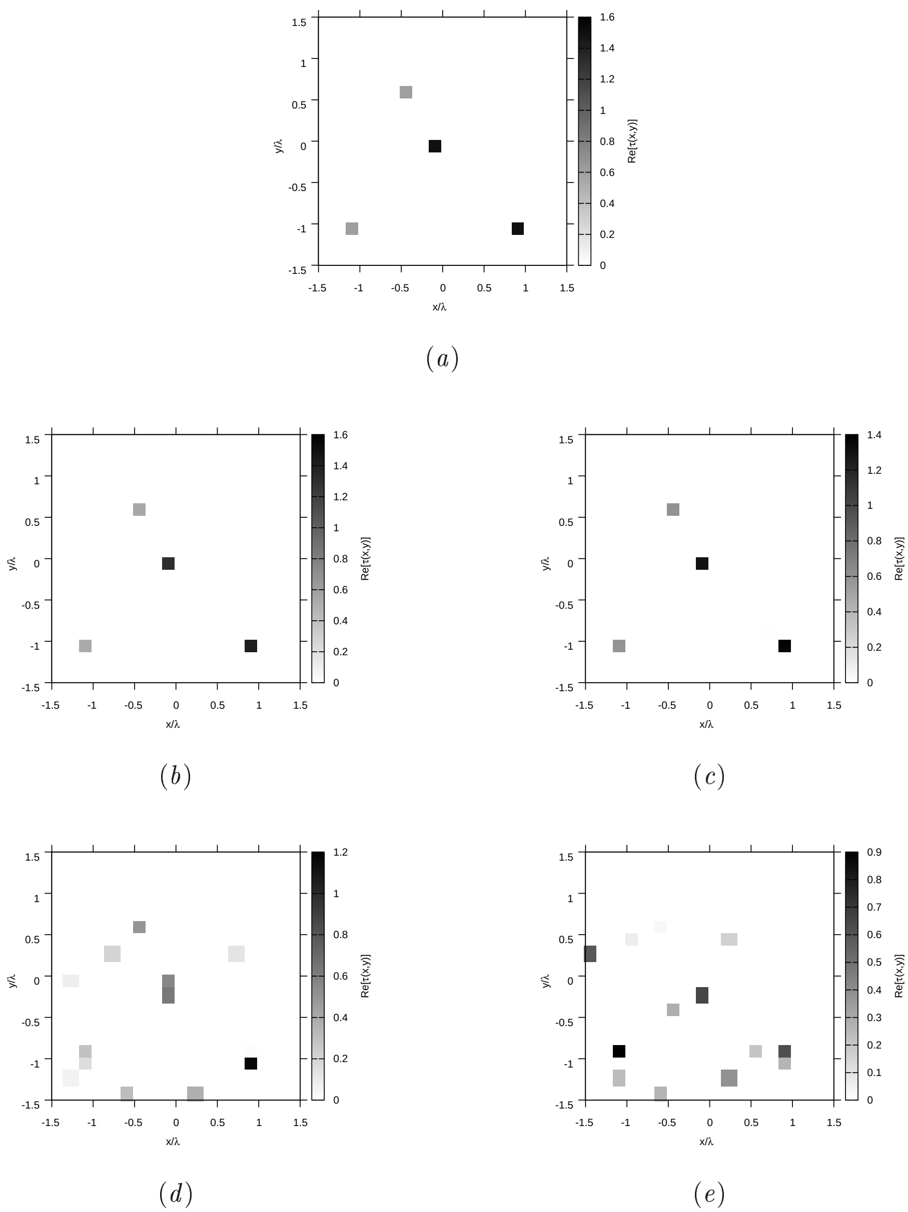

Figure 64. Actual object (a) and BCS reconstructed object for (b) Noiseless case, (c) $SNR = 20$ [dB] , (d) $SNR = 10$ [dB] , (e) $SNR = 5$ [dB].

Observations:

Ricostruzioni buone per i casi Noiseless e $SNR = 20\,dB$.

RESULTS: $\varepsilon_r = 3.0$

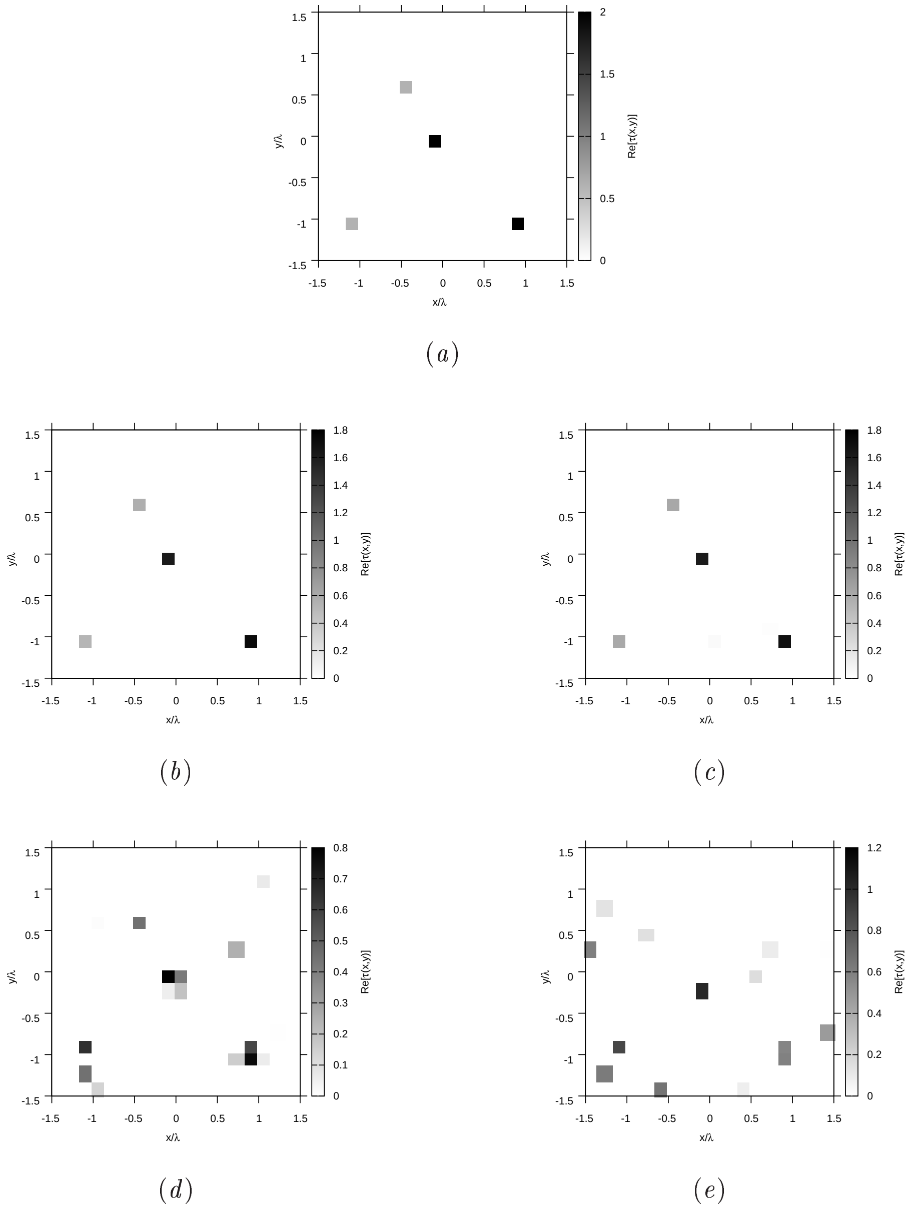

Figure 65. Actual object (a) and BCS reconstructed object for (b) Noiseless case, (c) $SNR = 20$ [dB] , (d) $SNR = 10$ [dB] , (e) $SNR = 5$ [dB].

Observations:

Ricostruzioni buone per i casi Noiseless e $SNR = 20\,dB$.

RESULTS: Error Figures

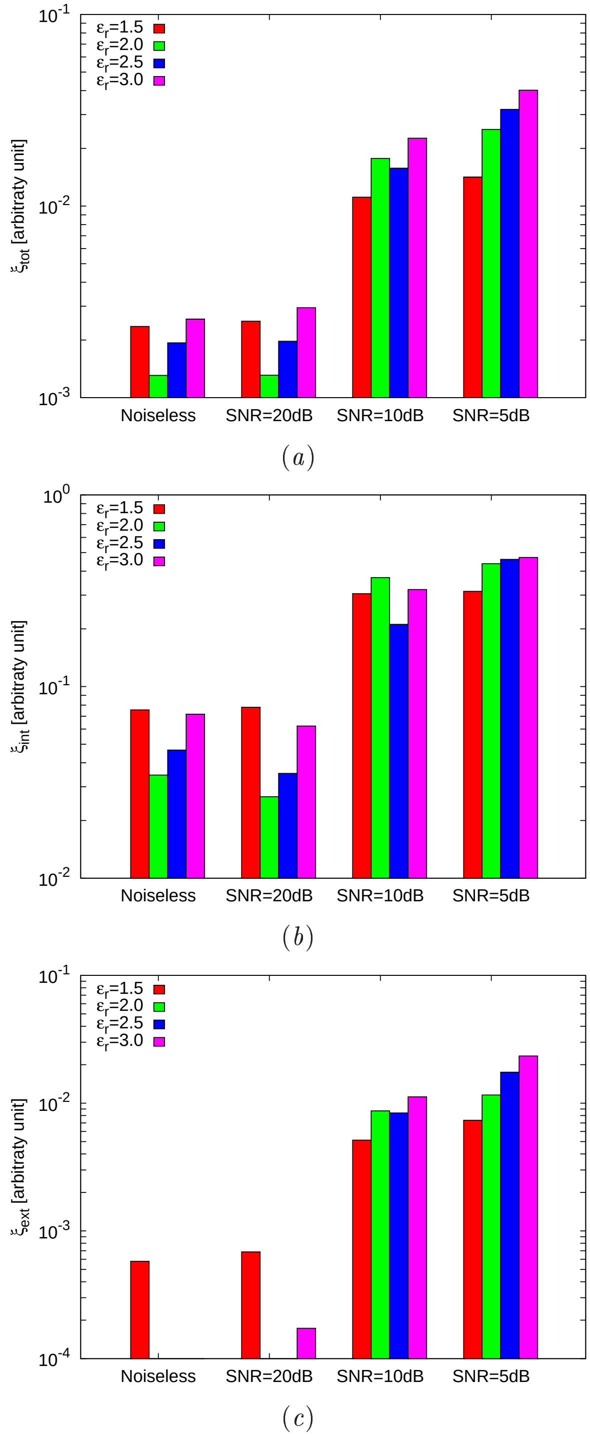

Figure 66. Behaviour of error figures as a function of ε_r, for different SNR values: (a) total error ξ_{tot}, (b) internal error ξ_{int}, (c) external error ξ_{ext}.

References

[1] E. J. Candes and M. B. Wakin, “An introduction to compressive sampling”, *IEEE Signal Processing Magazine*, vol. 25, no. 2, pp. 21-30, March 2008.

[2] S. Ji, Y. Xue, and L. Carin, “Bayesian compressive sampling”, *IEEE Trans. on Signal Processing*, vol. 56, no. 6, pp. 2346-2356, June 2008.

[3] R. F. Harrington, *Field computation by moment methods*, New York: IEEE Press, 1993.

[4] J. H. Richmond, “Scattering by a dielectric cylinder of arbitrary cross shape”, *IEEE Trans. Antennas Propagat.*, vol. AP-13, no. 3, pp. 334-341, May 1965.

[5] M. Slaney, A. C. Kak, and L. E. Larsen, “Limitations of imaging with first-order diffraction tomography”, *IEEE Trans. on Microwave Theory and Techniques*, vol. MTT-32, no. 8, pp. 860-874, Aug. 1984.

[6] L. Poli, G. Oliveri, and A. Massa, "Imaging sparse metallic cylinders through a Local Shape Function Bayesian Compressive Sensing approach," Journal of Optical Society of America A, vol. 30, no. 6, pp. 1261-1272, 2013.

[7] F. Viani, L. Poli, G. Oliveri, F. Robol, and A. Massa, "Sparse scatterers imaging through approximated multitask compressive sensing strategies," Microwave Opt. Technol. Lett., vol. 55, no. 7, pp. 1553-1558, Jul. 2013.

[8] L. Poli, G. Oliveri, P. Rocca, and A. Massa, "Bayesian compressive sensing approaches for the reconstruction of two-dimensional sparse scatterers under TE illumination," IEEE Trans. Geosci. Remote Sensing, vol. 51, no. 5, pp. 2920-2936, May. 2013.

[9] L. Poli, G. Oliveri, and A. Massa, "Microwave imaging within the first-order Born approximation by means of the contrast-field Bayesian compressive sensing," IEEE Trans. Antennas Propag., vol. 60, no. 6, pp. 2865-2879, Jun. 2012.

[10] G. Oliveri, P. Rocca, and A. Massa, "A bayesian compressive sampling-based inversion for imaging sparse scatterers," IEEE Trans. Geosci. Remote Sensing, vol. 49, no. 10, pp. 3993-4006, Oct. 2011.

[11] G. Oliveri, L. Poli, P. Rocca, and A. Massa, "Bayesian compressive optical imaging within the Rytov approximation," Optics Letters, vol. 37, no. 10, pp. 1760-1762, 2012.

[12] L. Poli, G. Oliveri, F. Viani, and A. Massa, "MT-BCS-based microwave imaging approach through minimum-norm current expansion," IEEE Trans. Antennas Propag., in press. doi:10.1109/TAP.2013.2265254

[13] S. C. Hagness, E. C. Fear, and A. Massa, "Guest Editorial: Special Cluster on Microwave Medical Imaging", IEEE Antennas Wireless Propag. Lett., vol. 11, pp. 1592-1597, 2012.

[14] G. Oliveri, Y. Zhong, X. Chen, and A. Massa, "Multi-resolution subspace-based optimization method for inverse scattering," Journal of Optical Society of America A, vol. 28, no. 10, pp. 2057-2069, Oct. 2011.

[15] A. Randazzo, G. Oliveri, A. Massa, and M. Pastorino, "Electromagnetic inversion with the multiscaling inexact-Newton method - Experimental validation," Microwave Opt. Technol. Lett., vol. 53, no. 12, pp. 2834-2838, Dec. 2011.

[16] G. Oliveri, L. Lizzi, M. Pastorino, and A. Massa, "A nested multi-scaling inexact-Newton iterative approach for microwave imaging," IEEE Trans. Antennas Propag., vol. 60, no. 2, pp. 971-983, Feb. 2012.

[17] G. Oliveri, A. Randazzo, M. Pastorino, and A. Massa, "Electromagnetic imaging within the contrast-source formulation by means of the multiscaling inexact Newton method," Journal of Optical Society of America A, vol. 29, no. 6, pp. 945-958, 2012.

[18] M. Benedetti, D. Lesselier, M. Lambert, and A. Massa, "Multiple shapes reconstruction by means of multi-region level sets," IEEE Trans. Geosci. Remote Sensing, vol. 48, no. 5, pp. 2330-2342, May 2010.

[19] M. Benedetti, D. Lesselier, M. Lambert, and A. Massa, "A multi-resolution technique based on shape optimization for the reconstruction of homogeneous dielectric objects," Inverse Problems, vol. 25, no. 1, pp. 1-26, Jan. 2009.

[20] M. Donelli, D. Franceschini, P. Rocca, and A. Massa, "Three-dimensional microwave imaging problems solved through an efficient multi-scaling particle swarm optimization," IEEE Trans. Geosci. Remote Sensing, vol. 47, no. 5, pp. 1467-1481, May 2009.

[21] M. Benedetti, G. Franceschini, R. Azaro, and A. Massa, "A numerical assessment of the reconstruction effectiveness of the integrated GA-based multicrack strategy," IEEE Antennas Wireless Propag. Lett., vol. 6, pp. 271-274, 2007.

[22] P. Rocca, M. Carlin, G. Oliveri, and A. Massa, "Interval analysis as applied to inverse scattering," IEEE International Symposium on Antennas Propag. (APS/URSI 2013), Chicago, Illinois, USA, Jul. 8-14, 2012.

[23] L. Manica, P. Rocca, M. Salucci, M. Carlin, and A. Massa, "Scattering data inversion through interval analysis under Rytov approximation," 7th European Conference on Antennas Propag. (EuCAP 2013), Gothenburg, Sweden, Apr. 8-12, 2013.

[24] P. Rocca, M. Carlin, and A. Massa, "Imaging weak scatterers by means of an innovative inverse scattering technique based on the interval analysis," 6th European Conference on Antennas Propag. (EuCAP 2012), Prague, Czech Republic, Mar. 26-30, 2012.

[25] G. Oliveri and A. Massa, "Bayesian compressive sampling for pattern synthesis with maximally sparse non-uniform linear arrays," IEEE Trans. Antennas Propag., vol. 59, no. 2, pp. 467-481, Feb. 2011.

[26] G. Oliveri, M. Carlin, and A. Massa, "Complex-weight sparse linear array synthesis by Bayesian Compressive Sampling," IEEE Trans. Antennas Propag., vol. 60, no. 5, pp. 2309-2326, May 2012.

[27] G. Oliveri, P. Rocca, and A. Massa, "Reliable Diagnosis of Large Linear Arrays - A Bayesian Compressive Sensing Approach," IEEE Trans. Antennas Propag., vol. 60, no. 10, pp. 4627-4636, Oct. 2012.

[28] F. Viani, G. Oliveri, and A. Massa, "Compressive sensing pattern matching techniques for synthesizing planar sparse arrays" IEEE Trans. Antennas Propag., in press. doi:10.1109/TAP.2013.2267195

[29] M. Carlin, P. Rocca, G. Oliveri, F. Viani, and A. Massa, "Directions-of-Arrival Estimation through Bayesian Compressive Sensing strategies," IEEE Trans. Antennas Propag., in press.

[30] M. Carlin, P. Rocca, "A Bayesian compressive sensing strategy for direction-of-arrival estimation," 6th European Conference on Antennas Propag. (EuCAP 2012), Prague, Czech Republic, pp. 1508-1509, 26-30 Mar. 2012.

[31] M. Carlin, P. Rocca, G. Oliveri, and A. Massa, "Bayesian compressive sensing as applied to directions-of-arrival estimation in planar arrays", Journal of Electrical and Computer Engineering, Special Issue on "Advances in Radar Technologies", in press.